PCCP

PAPER

View Article Online
View Journal | View Issue

Cite this: *Phys. Chem. Chem. Phys.*, 2018, **20**, 25203

Photoelectron spectroscopy and thermochemistry of *o*-, *m*-, and *p*-methylenephenoxide anions†

Daniel J. Nelson, ‡[a] Wilson K. Gichuhi, §[a] Charles M. Nichols, ¶[a] Veronica M. Bierbaum, *[a] W. Carl Lineberger *[a] and Julia H. Lehman *[ab]

The anionic products following (H + H^+) abstraction from *o*-, *m*-, and *p*-methylphenol (cresol) are investigated using flowing afterglow-selected ion flow tube (FA-SIFT) mass spectrometry and anion photoelectron spectroscopy (PES). The PES of the multiple anion isomers formed in this reaction are reported, including those for the most abundant isomers, *o*-, *m*- and *p*-methylenephenoxide distonic radical anions. The electron affinity (EA) of the ground triplet electronic state of neutral *m*-methylenephenoxyl diradical was measured to be 2.227 ± 0.008 eV. However, the ground singlet electronic states of *o*- and *p*-methylenephenoxyl were found to be significantly stabilized by their resonance forms as a substituted cyclohexadienone, resulting in measured EAs of 1.217 ± 0.012 and 1.096 ± 0.007 eV, respectively. Upon electron photodetachment, the resulting neutral molecules were shown to have Franck–Condon active ring distortion vibrational modes with measured frequencies of 570 ± 180 and 450 ± 80 cm^{-1} for the *ortho* and *para* isomers, respectively. Photodetachment to excited electronic states was also investigated for all isomers, where similar vibrational modes were found to be Franck–Condon active, and singlet–triplet splittings are reported. The thermochemistry of these molecules was investigated using FA-SIFT combined with the acid bracketing technique to yield $\Delta_{acid}H^{\circ}_{298K}$ values of 341.4 ± 4.3, 349.1 ± 3.0, and 341.4 ± 4.3 kcal mol^{-1} for the *o*-, *m*-, and *p*-methylenephenol radicals, respectively. Construction of a thermodynamic cycle allowed for an experimental determination of the bond dissociation energy of the O–H bond of *m*-methylenephenol radical to be 86 ± 4 kcal mol^{-1}, while this bond is significantly weaker for the *ortho* and *para* isomers at 55 ± 5 and 52 ± 5 kcal mol^{-1}, respectively. Additional EAs and vibrational frequencies are reported for several methylphenyloxyl diradical isomers, the negative ions of which are also formed by the reaction of cresol with O^-.

Received 24th August 2018,
Accepted 20th September 2018

DOI: 10.1039/c8cp05403g

rsc.li/pccp

I. Introduction

Studies of radicals and diradicals are of interest to many diverse fields of chemistry, biology, and physics.[1–9] For instance, in one potent subset of anticancer drugs,[3] DNA strand cleavage leading to cell apoptosis can be initiated by the diradical *p*-benzyne, generated from the Bergman cyclization reaction of enediyne.[10] Due to their frequently unstable and short-lived nature, as well as their complicated electronic structure,[11–20] these types of diradicals are challenging to investigate both experimentally and theoretically. However, a thorough characterization of their thermodynamic and spectroscopic properties is an important step towards further understanding their role as reaction intermediates.

Studies of distonic radical ions, ions that have their radical site separated from their charge site, are also of interest to the scientific community.[21–35] Radical ions may react either as radicals or as ions, with their multifunctionality allowing them to contribute to a number of reaction schemes. Their initial study is largely due to the pioneering work of Kenttämaa and coworkers and their efforts towards understanding distonic radical cations in the gas phase,[34] although distonic radical anions have also been extensively explored.[23,26,29] As the study of these radical ions continues, they have been shown to be relevant in reaction mechanisms, often in zwitterionic chemistry, with a famous example being the McLafferty rearrangement of molecular ions in carbonyl compounds.

In some early work, distonic radical anions were studied with electron spin resonance spectroscopy.[22] However, these initial

[a] *JILA and the Department of Chemistry, University of Colorado, Boulder, CO 80309, USA. E-mail: Veronica.Bierbaum@colorado.edu, J.Lehman@leeds.ac.uk, Carl.Lineberger@colorado.edu*
[b] *School of Chemistry, University of Leeds, Leeds LS2 9JT, UK*

† Electronic supplementary information (ESI) available: Relevant additional photoelectron spectra, photoelectron angular anisotropy information, and calculated normal mode vectors are presented. See DOI: 10.1039/c8cp05403g

‡ Present address: Leybold, 5700 Mellon Rd, Export, PA 15632, USA.
§ Present address: Department of Chemistry, Tennessee Tech University, Cookeville, TN 38505, USA.
¶ Present address: Agilent Technologies, Santa Clara, CA 95051, USA.

studies were limited to distonic radical anions and/or diradicals that were long-lived in the condensed phase, with lifetimes on the order of minutes to hours. Later, both diradicals and distonic radical anions became a focus of gas phase studies, particularly within the mass spectrometry field. Both electrospray ionization[30] and gas phase deprotonation reactions, such as using flowing afterglow – selected ion flow tube (FA-SIFT) mass spectrometry,[28] have been instrumental in providing more information on the structure and energetics of these reaction intermediates. The latter technique, which involves reacting O^- with a neutral molecule of interest, is used in this study.

Time of flight (TOF) mass spectrometry, Fourier transform ion cyclotron resonance mass spectroscopy, and collision induced dissociation have all been utilized to study these types of molecules and anions.[22,23,34] Anion photoelectron spectroscopy (PES) has been a particularly advantageous technique in characterizing distonic radical anions and their corresponding neutral diradicals. By starting with the open shell distonic radical anion and photodetaching an electron, transitions to both the singlet and triplet electronic states of the neutral diradical can be observed. Thus, anion PES has the potential to yield a wealth of information, including details of the electronic structure (such as the electron affinity and singlet–triplet splitting) and vibrational frequencies of the neutral diradical.

This study investigates the *ortho*, *meta*, and *para* isomers of methylphenol, also known as cresol, following their reaction with O^- in the gas phase. The abstraction of $(H + H^+)$ by O^- will be shown to primarily produce the distonic radical anions *o*-, *m*-, and *p*-methylenephenoxide. Cresols themselves are critical reagents in many organic syntheses and in a large number of industrial applications.[36–45] Much of their behavior is well understood, and thus they are used as model systems in studies ranging from catalysis to ionic liquids. While a wealth of information exists on cresols, including our own work on methylphenoxide anions and methylphenoxyl radicals,[46] methylenephenoxides are not yet well understood and present an opportunity to study distonic radical anions and diradicals by way of photodetachment. This work is a joint effort across three different experimental setups, using both pulsed and continuous anion PES, as well as FA-SIFT mass spectrometry in conjunction with the acid bracketing procedure.[47] This combined effort yields information on the electron affinities (EAs), singlet–triplet splittings, and several vibrational frequencies of the neutral methylenephenoxyl molecules, along with deprotonation enthalpies of the methylenephenol radicals. This information is used in conjunction with a thermodynamic cycle to derive the O–H bond dissociation energies for the methylenephenol radicals.

II. Experimental methods

Chemical samples

Samples of *o*-, *m*-, and *p*-methylphenol were obtained from Sigma-Aldrich Inc. (≥98% pure). Selectively deuterated samples of 3,4,5,6-d_4,OD-*o*-methylphenol and methyl-d_3-*m*-methylphenol were purchased from CDN Isotopes, Inc. (≥98% pure), while 2,3,5,6-d_4,OD-*p*-methylphenol was purchased from Sigma-Aldrich Inc. (≥98% pure). Acids for the bracketing experiments using the FA-SIFT instrument were purchased from Sigma-Aldrich Inc. with the exception of phenol (Mallinckrodt Pharmaceuticals Inc.). The acids and their given purities are as follows: *p*-trifluoromethylphenol (≥97%), 3-mercaptopropionic acid (≥99%), *o*-chlorophenol (≥99%), *p*-fluorophenol (≥99%), propionic acid (≥99.5%), acetic acid (≥99%), phenol (≥99%), 2,2,3,3,3-pentafluoro-1-propanol (≥97%). All of the chemicals were used without further purification. The low vapor pressure of many of these compounds necessitated that they be gently heated (~40 °C) for sufficient gas-phase quantities to be introduced into the instrument.

Instrumentation

Three distinct experimental apparatus are utilized in the present study. The first instrument is an FA-SIFT mass spectrometer. The second instrument is a pulsed photoelectron spectrometer (pulsed PES), using a dual pulsed valve plasma entrainment ion source, pulsed nanosecond laser, and velocity map imaging detector. The third instrument is a continuous photoelectron spectrometer (cw PES) fitted with a flowing afterglow ion source, cw Ar-ion laser, and hemispherical energy analyzer. All three of these instruments have been discussed in detail previously,[48–53] so only brief descriptions follow.

1. FA-SIFT instrument. The FA-SIFT instrument produces ions using a flowing helium plasma, made by electron impact *via* a filament discharge.[49] For these studies, O^- is generated *via* ionization and decomposition of N_2O. As a strong base ($\Delta_{acid}H^\circ_{298K}(OH) = 382.60 \pm 0.07$ kcal mol^{-1}[54]), the O^- radical anion is capable of abstracting either H^+ from methylphenol, resulting in an anion and hydroxyl radical, or it can remove both a hydrogen atom and a proton, to produce an anion and a water molecule. The methylphenol reactant is added downstream of the O^- formation region, and the products and reactants remain in ~0.3 Torr He for several milliseconds before being extracted through a 1 mm orifice into a differentially pumped region (~10^{-6} Torr). The anionic products are then mass selected with a quadrupole mass filter and subsequently entrained in the reaction flow tube with a laminar flow of He (~0.5 Torr). There are gas inlets at regular intervals along the flow tube where neutral reagents may be added to study the thermochemistry of gas phase ion-neutral reactions. In this study, neutral acids with known deprotonation enthalpies are introduced in order to monitor their reactivity with the anions of interest. At the downstream end of the flow tube, all anions are extracted into a differentially pumped chamber (~10^{-7} Torr), mass analyzed with a triple quadrupole mass analyzer, and detected with a Channeltron electron multiplier.

The acid bracketing technique used here is summarized as follows.[47] The mass selected methylenephenoxides are reacted with neutral acids of known deprotonation enthalpy (reference acids) in the laminar flowing helium. Since the anions are Lewis bases, a collision with a neutral acid will likely result in a proton transfer from the acid to the base if the proton affinity of

the base is larger than the deprotonation enthalpy of the acid. If a reaction takes place, a decrease in the parent anion signal and the appearance of new anion products is observed. A rapid proton transfer reaction with a reference acid indicates an exothermic reaction, whereas no change in anion signal is assumed to indicate an endothermic reaction. Using a variety of reference acids, the trends in reactivity can be observed. The deprotonation enthalpy of the conjugate acid of methylenephenoxide (*i.e.* methylenephenol) lies between the values of the two reference acids wherein the proton transfer reaction changed from endothermic to exothermic.

While performing experiments with the FA-SIFT, it became necessary to inject CO_2 clustered with the ions of interest into the flow tube region; this produced greater signal due to decreased diffusive loss of ions in the source. This procedure should not affect the chemistry observed. A wider mass window was used to inject the ion-CO_2 cluster and higher order clusters; the injection energy of 30–70 V is more than sufficient to dissociate the clusters into the parent ion and CO_2, whereupon the parent ion can react unencumbered in the flow tube.

2. Pulsed PES instrument. In the pulsed PES instrument,[53] the anions of interest are synthesized in a dual pulsed valve plasma entrainment source utilizing the same reaction of methylphenol with O^-. This source uses two pulsed General Valves placed perpendicular to each other. The first is the primary supersonic expansion (1.65 bar, ~1% methylphenol in Ar), while the other valve is designated the side valve (3.38 bar, 30% O_2 balance Ar). For normal daily operation, the side valve tension is adjusted such that the side gas expansion produces ~10% of the total pressure rise in the source vacuum chamber. The side valve has a pulsed parallel plate discharge at the valve exit ($\Delta V \sim -2000$ V).[51] This generates a plasma which is entrained in the primary supersonic expansion. The dominant anion generated therein, O^-, then undergoes reactions with the methylphenol isomer of interest contained in the main expansion, generating products which are collisionally cooled with Ar. The most thermodynamically favorable products from the reaction of O^- with methylphenol were observed, as well as other anionic products (see Results).

Following their initial formation, the anions are steered into a Wiley–McLaren TOF mass spectrometer by a pulsed extraction plate, where the ions are temporally separated by their mass to charge ratio (m/z) and spatially focused into the center of a Velocity Map Imaging (VMI) interaction region.[52] A nanosecond laser pulse is timed to intercept the anion m/z of interest, photodetaching electrons. The light sources used to obtain the spectra reported here are the second and third harmonic of a Nd:YAG laser, with photon energies of 2.330 and 3.494 eV, respectively. The three-dimensional distributions of photodetached electrons are velocity mapped onto a two-dimensional position sensitive microchannel plate detector coupled to a phosphor screen, which is then imaged by a CCD camera. This photoelectron image is reconstructed into the original three-dimensional velocity distribution utilizing an inverse Abel transform. This is then converted to a one-dimensional electron speed distribution. Both steps are performed using the BASEX program.[55] Finally an electron Kinetic Energy (eKE) distribution is generated by means of a Jacobian transformation. This spectrum is converted to an electron Binding Energy (eBE) distribution by subtracting the eKE from the laser photon energy (eBE = $h\nu$ − eKE), yielding the reported PES.

The VMI spectrometer has a spectral resolution that is a function of eKE; the resolution decreases with increasing eKE. The experimental resolution is determined by the eKE and the FWHM of peaks in a PES due to single transitions. In all cases presented in this work, the PES of S^- was used to determine the instrument resolution as a function of eKE, as well as to calibrate the energy scale.[56,57] Typically, the resolution is ~2–3% (resolution ~ FWHM/eKE).

3. Continuous PES instrument. In the continuous PES instrument, the ions of interest are generated in a flowing-afterglow He (~0.5 Torr) plasma, similar to that used in the FA-SIFT instrument. Molecular oxygen is added to this plasma, which generates O^-. Each methylphenol isomer is added through a gas inlet immediately after the O^- radical anions are generated. The products from this reaction remain in ~0.5 Torr of He for several milliseconds, thermally equilibrating with the walls of the chamber (300 K), before being extracted through a 1 mm orifice into a low pressure differentially pumped region (~10^{-6} Torr). It is important to note that the reactants and products undergo multiple collisions, and hence the nascent product distributions arising from the reaction of O^- and the methylphenols (*i.e.* the products of a single collision between an O^- and methylphenol molecule) are not necessarily the products observed in the PES.

After being produced and extracted into the differentially pumped region, the anionic products are accelerated to 735 eV, mass selected with a Wein velocity filter ($m/\Delta m \sim 60$), before being slowed to 35 eV and intersected with a fixed frequency argon ion laser ($h\nu$ = 3.40814 eV), thereby photodetaching electrons from the mass-selected ions of interest. A small solid angle of these electrons is gathered in a direction perpendicular to both the ion and laser beams, and the kinetic energy is measured using a hemispherical electron energy analyzer. The laser radiation is linearly polarized at the magic angle (54.7°), ensuring that the gathered photoelectrons are directly proportional to the anion's photoelectron detachment cross section.[58] The laser has an output power of ~1 Watt at 364 nm, which is coupled into the chamber *via* a build-up cavity locked to the laser cavity, increasing the circulated in-cavity power to ~100 Watts.

The collected PES are calibrated to the PES of O^- and O_2^-.[59,60] This procedure provides an absolute linear energy scale and corrects for a nonlinear energy scale distortion with a minor (0.7%) compression factor. The calibration spectrum of O^- also allows for a measurement of the instrument's resolution, 10 meV. This is obtained by measuring the full-width-half-maximum (FWHM) of the $O(^3P_2) + e^- \leftarrow O^-(^2P_{3/2})$ transition. Because this peak results from a single (atomic) transition, its FWHM is a good approximation of the instrument resolution.

Error analysis

Throughout this work, errors in reported peak positions in the PES are typically on the order of 1 meV or less. This error is due

to several factors: the statistical error in fitting the peaks to Gaussian functions to obtain the peak center, the uncertainty in the absolute energy scale, and the number of independent measurements. When reporting a particular transition energy, which uses the energy difference between peaks in a spectrum, the previous errors are taken into account and are combined with the uncertainty associated with the offset of the actual transition compared to the peak center. This uncertainty can be smaller or comparable to the aforementioned errors if only a single vibronic transition is the major contributor to the peak. However, if there are multiple transitions under the peak envelope, which can sometimes manifest itself as a non-Gaussian peak or a peak possessing a FWHM wider than would be predicted by the experimental resolution at that eKE, it can be as much as the Half-Width-at-Half-Maximum (HWHM) of the peak. The peaks presented in all reported spectra are broader than the instrument resolution and always arise from multiple transitions with significant transition intensity. Hence, this latter error dominates the reported uncertainty.

III. Theoretical methods

The BMK/6-311+G(3df,2p) method is used to calculate the vibrational normal modes of the anions and neutrals, which are subsequently employed in the computation of the Franck–Condon (FC) factors. This level of theory has previously been shown to work well with distonic radical anions and their corresponding neutrals, and has been benchmarked against experiment and other high levels of theory for a range of species.[24,25] The CBS-QB3 composite method is used to determine accurate energies of the anions and neutrals in order to calculate adiabatic EAs, singlet–triplet splittings, and $\Delta_{acid}H^{\circ}_{298K}$ of the protonated form of all the anions of interest. Where relevant, TDDFT is used to calculate energies, geometries, and vibrational frequencies for electronically excited singlet and triplet states of the neutral species. All of the electronic structure, normal mode, and thermochemical calculations are carried out using the Gaussian 09 program package,[61] while the FC factors are calculated using the PESCAL program.[50]

To simulate the experimental spectra, PESCAL calculates the positions of all possible vibrational transitions and the Franck–Condon factor associated with each transition. This information, combined with a 200 K Maxwell–Boltzmann distribution of population in the initial anionic states for the pulsed PES instrument (300 K for the continuous PES instrument), generates a stick spectrum. These sticks are then convolved with Gaussian functions whose integrated area is equal to the calculated transition intensity (FC factor) and whose FWHM is commensurate with the instrument resolution to yield the final simulated spectra. PESCAL utilizes Duschinsky rotation matrices and displacement vectors to match the initial state normal mode coordinates to the final state normal mode coordinates such that the FC integrals may be evaluated *via* the Sharp–Rosenstock–Chen method.[62–65] The calculated FC factors make use of the harmonic oscillator approximation, with no anharmonic corrections or cross-mode couplings.

IV. Results

The reaction of O^- with methylphenol could, in theory, produce a number of different anionic products. Deuteration studies were employed to verify which products were dominant for further investigation using the PES techniques. Fig. 1 displays the mass spectra collected with the FA-SIFT instrument, showing the range of products from the reaction of selectively deuterated

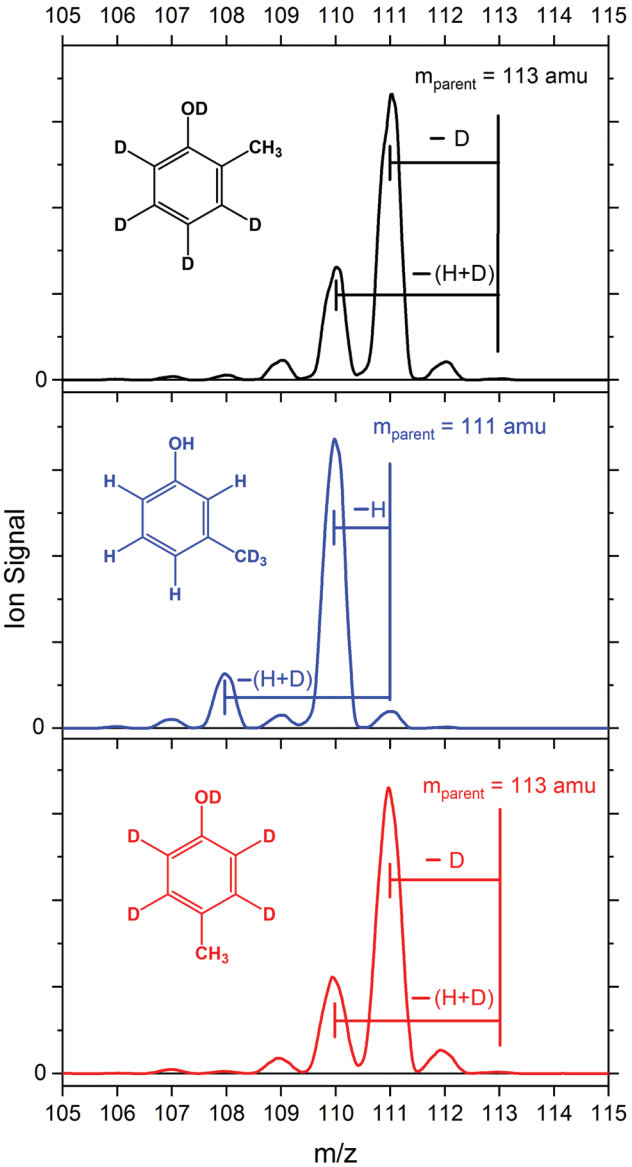

Fig. 1 Mass spectra collected with the FA-SIFT instrument of selectively deuterated *o*- (black), *m*- (blue), and *p*- (red) cresols reacted with O^-. In each panel, the parent cresol structure is shown and a vertical line indicates the parent mass. For each isomer, deprotonation from the O site is the largest observed product channel, while the next largest channel is (H + D) loss from the hydroxyl and methyl groups. More details may be found in the text.

methylphenols with O^-. In each case, the primary product arises from deprotonation of the hydroxyl group, generating methylphenoxide. This product has been previously studied *via* PES,[46] where the photodetachment from methylphenoxide produces signal that spans from approximately 2.1 to 2.7 eV. The small peaks that are 1 amu higher than the most abundant peak in each spectrum represent the anions containing one carbon-13 atom.

The next most abundant product evident in the mass spectra is a loss of both H and D from the parent methylphenol. There are two possibilities for the loss of m/z = 3 from the partially deuterated methylphenol: either loss from the hydroxyl group plus loss from the methyl group, or loss from methyl group plus loss from the ring. This second option is less likely because sequential abstraction from the methyl group followed by the ring is either thermoneutral or endothermic (CBS-QB3). This is in contrast to the hydrogens found on the methyl group of methylphenoxide, for which hydrogen abstraction is exothermic using O^-, OH, or OH^-. Assuming this exothermic radical-ion reaction does not have a barrier to reaction, the anionic product from the loss of both H and D is expected to be an isomer of methylenephenoxide (Fig. 2, panel A).

There are also some smaller peaks evident in the mass spectrum, such as the loss of m/z = 4 (*ortho* and *para*) and the loss of m/z = 2 (*meta*). A loss of m/z = 2 for the *meta* isomer is likely due to deuterium abstraction from the methyl group, which was seen by Nelson *et al.*[46] However, a loss of m/z = 4 from *ortho* and *para* is most likely deuterium loss from the hydroxy group plus deuterium loss from the ring, and is also a possible product for the *meta* isomer. This is a exothermic process for all three isomers (CBS-QB3), regardless of the site of the ring loss. This will result in the production of methylphenyloxide anions (Fig. 2, panel B).

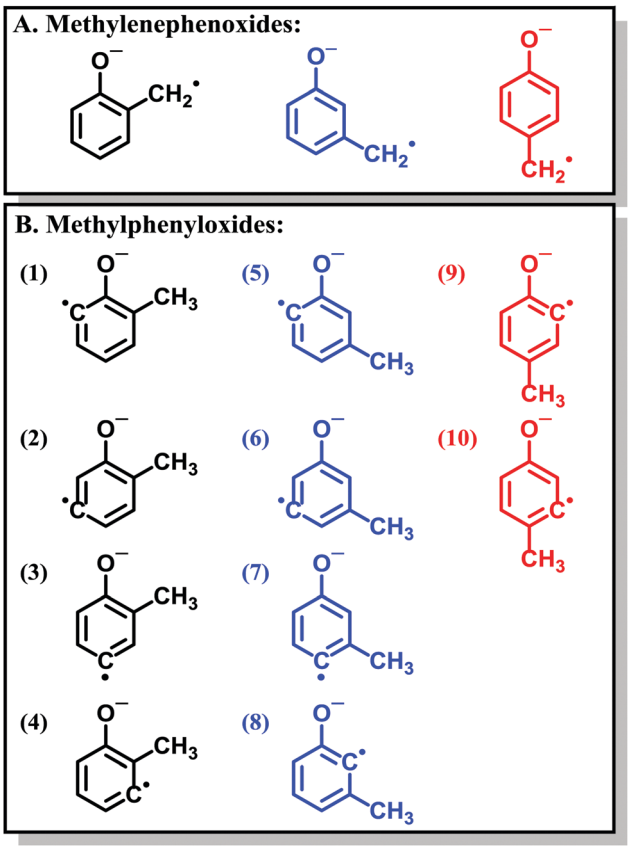

Fig. 2 Possible anion isomers, based on results from isotope studies (Fig. 1) and thermodynamic calculations, formed following the reaction of O^- with *o*- (black), *m*- (blue), and *p*- (red) methylphenol, resulting in the abstraction of (H + H^+). The anions are split into two categories: methylenephenoxides (panel A) and methylphenyloxides (panel B).

Electronic structure calculations and FC simulations were carried out for other possible non-deuterated structural isomers with the same mass (m/z = 106) and were compared to the experimental PES. These studies were done in an effort to rule out possible proton transfer, ring opening, ring rearrangement, or other reactions giving rise to any of the peaks seen in the spectra. No photoelectron signatures belonging to these other structural isomers were positively identified in the spectra. However, even in combination with the deuteration study (Fig. 1), this cannot completely rule out the existence of such anions in the experiment.

Prior to examining the PES, it is useful to consider what one might expect from the PES of the m/z = 106 anions resulting from the reaction of O^- with methylphenol, specifically: the EAs of the neutral isomers, the possibility of observing excited electronic states, and the normal mode vibrations excited upon photodetachment. For methylenephenoxide anions (Fig. 2, panel A) and methylphenyloxide anions (Fig. 2, panel B), it is expected that the negative charge would primarily be localized on the oxygen. Similar substituted phenoxide anions have been studied previously, such as methylphenoxide.[46] The methylphenoxyl radical was found to have an EA of approximately 2 eV, which is a good initial estimate of what might be expected for methylenephenoxyl or methylphenyloxyl radicals. However, the *ortho* and *para* isomers of the neutral methylenephenoxyl diradicals have a significantly more stable resonance form in their singlet ground electronic state, specifically forming a substituted cyclohexadienone. For the *ortho* isomer, it is 6-methylene-2,4-cyclohexadien-1-one, while for the *para* isomer, it is 4-methylene-2,5-cyclohexadien-1-one. These stable resonance forms of the singlet ground electronic states would lower the energy of the neutral relative to the anion, resulting in a lower EA, likely to be on the order of 1 eV.

With sufficient photon energy, both the ground and the lowest lying excited electronic states of the neutrals could be accessed. Considering the PES spin selection rule $\Delta S = \pm\frac{1}{2}$, detachment from the doublet ground electronic state of the anion would result in either singlet or triplet multiplicity for the electronic states of the neutral. If the singlet–triplet splitting for these radicals is less than approximately 2 eV, a photon energy of 3.494 eV might be sufficient to observe the origin of the excited electronic state of the neutral. Note that the above stable cyclohexadienone resonance forms for *ortho* and *para* would not be possible in their triplet excited states, and these would instead be neutral methylenephenoxyl diradicals.

The added electron primarily localized on the oxygen moiety results in a lengthening of the ring structure along this axis of

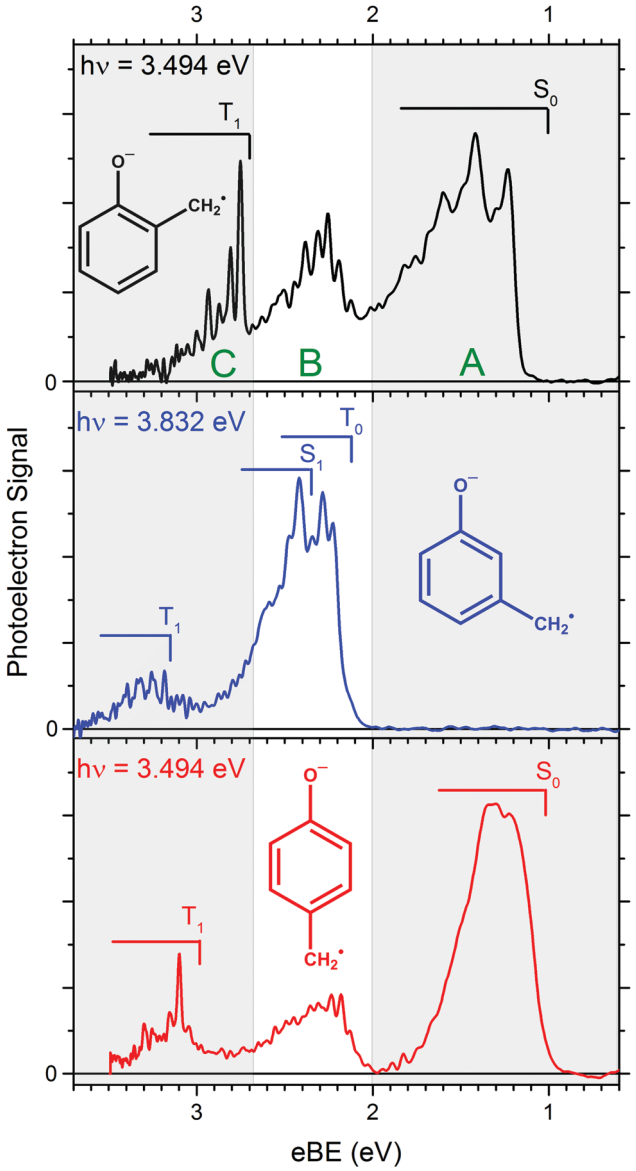

Fig. 3 Photoelectron spectra of the m/z = 106 anions produced from reaction of O^- with three isomers of methylphenol. Spectra were taken with the pulsed PES instrument with a photon energy of 3.494 eV or 3.832 eV. The spectra are highlighted to differentiate three regions, labelled A, B, and C. The inset methylenephenoxide anion structure shows the primary isomer anion responsible for the observed PES in regions A and C (for *ortho* and *para*) and region B and C (*meta*). The electronic states of the dominant neutral molecules accessed from electron photodetachment of the methylenephenoxide anion are also labeled.

the molecule relative to the structure of the neutral. Thus, upon photodetachment, primarily ring distortion vibrations are likely to be observed. This was also the case for photodetachment from methylphenoxide.

Fig. 3 shows the PES of the m/z = 106 anions resulting from the reaction of O^- with *o*-, *m*-, and *p*-methylphenol, obtained utilizing the pulsed PES instrument. For *ortho* and *para* isomers, a considerable amount of activity may be seen spanning the spectra from ~1 eV through to the photon energy, 3.494 eV. The activity can largely be split into three regions based on eBE: (A) 1–2 eV; (B) 2–2.7 eV; (C) 2.7–3.494 eV, as denoted by the shaded areas in Fig. 3. The largest integrated intensity belongs to the lowest eBE peaks, spanning approximately 1–2 eV, or region A. This is slightly lower eBE than what is expected based on initial estimates of the EA(methylenephenoxyl), but it is consistent with the revised estimate of the EA based on the resonance form of the substituted cyclohexadienone. The transitions in regions A, B, and C for the *ortho* and *para* isomers will be discussed further below.

The *meta* isomer shows a distinctly different PES, with no signal in region A and the majority of photoelectron signal in region B. This is more consistent with the initial predictions of the EA(methylenephenoxyl). Because it exhibits significant differences from the *ortho* and *para* isomer PESs, the *meta* isomer will be discussed separately.

Region A: photodetachment to the S_0 state of *o*- and *p*-methylenephenoxyl

In order to obtain accurate EAs for the *ortho* and *para* isomers, higher resolution spectra of region A are necessary. Recall that the resolution of the VMI spectrometer improves as the eKE is decreased. While the transition to S_0 might appear broad in Fig. 3, higher resolution can be achieved by either changing the photon energy used in the pulsed PES instrument, or utilizing the constant energy resolution inherent to the cw PES instrument. This latter option was chosen, and the results are shown in Fig. 4, where the experimental data are shown as black and red traces, and the theoretical results are shown as the purple sticks (FCFs) and the green curves (convolutions). The higher resolution data reveal structured spectra, including clearly defined peaks that can be attributed to transitions from the anion to the neutral S_0 state. The origin peak is close to 1 eV, as expected for the EA of methylenephenoxyl radicals. The PES for both the *ortho* and *para* isomers show a series of peaks spaced by intervals of approximately 500 cm^{-1}. As mentioned previously, this is expected to be related to the ring distortion vibrational modes.

In order to further analyze the spectra, a comparison between theory and experiment is instructive. For both isomers, there is good agreement between the experimental results and the theoretical predictions, further confirming the assignment of these PES as detachment from *o*- and *p*-methylenephenoxide to form the S_0 state of the corresponding neutral. For *o*-methylenephenoxide (top panel), peak A is predicted to be due primarily to the transition from the anion vibronic ground state to the neutral vibronic ground state, *i.e.* the EA. The center of peak A is measured to be 1.217 ± 0.001 eV, leading to a measurement of the EA = 1.217 ± 0.012. Similarly, peak A for the *para* isomer (lower panel, Fig. 4) is predicted to be dominated by the origin transition (EA), with its peak center located at 1.096 ± 0.001 eV, and thus the EA is measured to be 1.096 ± 0.007 eV. It is instructive to note that for both *ortho* and *para* isomers, while the origin transition contributes the largest predicted transition intensity to peak A, many other transitions also contribute, such as sequence bands and low frequency hot bands. These other transitions are distributed non-symmetrically about the

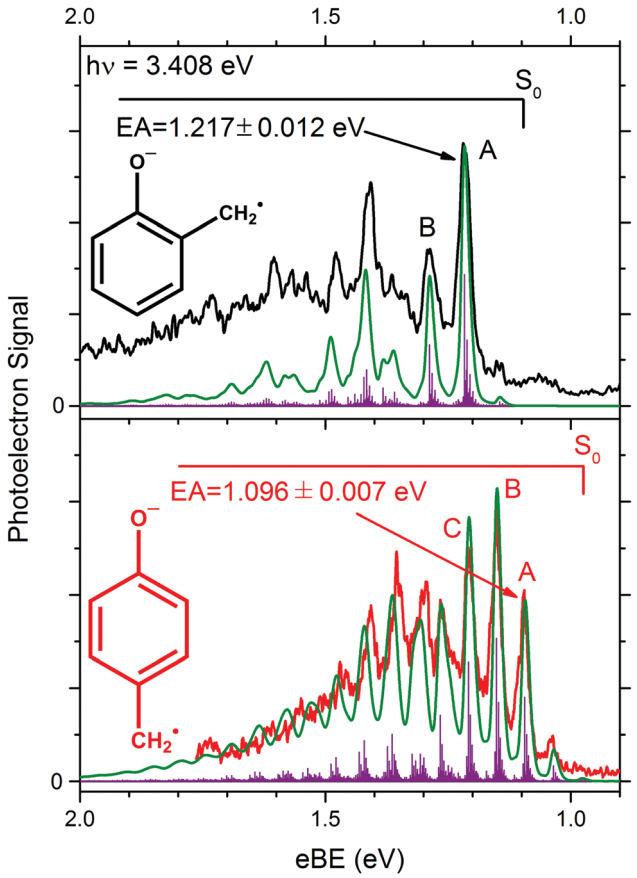

Fig. 4 Photoelectron spectra of the *o*- and *p*-methylenephenoxide anions obtained with the continuous PES instrument utilizing a photon energy of 3.408 eV are shown in the black and red traces, respectively. This instrument has a constant spectral resolution of 10 meV. The calculated transitions and their corresponding Franck–Condon intensities are represented by purple sticks, while their convolutions with experimental resolution are shown in green.

peak center, giving rise to a non-Gaussian shape and a peak width that is significantly broader than the experimental resolution. Thus, the peak HWHM is used in the error analysis and is the dominant contributor to the error on the EA.

The remainder of the PES for both isomers shows good agreement between theory and experiment. In both cases, the structure present in the spectra matches transitions from the anion to vibrationally excited states in the neutral S_0 state, primarily involving ring distortion vibrational modes as expected. The energy differences between the EA and other peaks within this electronic manifold allow for measurement of the vibrational transition energies of the neutral.

For the *o*-methylenephenoxide PES (top panel of Fig. 4), Peak B is located 571 ± 10 cm^{-1} relative to the center of peak A. Peak B is predicted to have arisen primarily from a transition to an excited ring distortion vibrational mode, as was expected. The peak spacing relative to the EA yields an experimental measure of the neutral vibrational transition 29_0^1 = 570 ± 180 cm^{-1}, as compared with the predicted value of 574 cm^{-1}. Due to experimental resolution and predicted spectral congestion, other peaks could not be positively assigned to transitions of any single vibrational mode of the neutral.

For the PES of *p*-methylenephenoxide (bottom panel of Fig. 4), peaks B and C have peak centers 452 ± 10 and 899 ± 10 cm^{-1}, respectively, higher in binding energy relative to peak A. The intensities of peaks B and C are primarily attributed to excitations of one ring distortional vibrational mode (ν_{32}) with a calculated harmonic frequency of 462 cm^{-1}. Thus, the transitions involving this mode are experimentally measured to be 32_0^1 = 450 ± 80 cm^{-1} and 32_0^2 = 900 ± 140 cm^{-1}. Peaks higher in binding energy than peak C are due to several transitions that include combination bands of a variety of ring distortion vibrational modes (~500 cm^{-1}) as well as modes that incorporate ring distortion motion with C–O stretch motion (~1500 cm^{-1}). Since these peaks are not clearly dominated by only one or two transitions, further assignments are again not appropriate. See the ESI† for the normal mode vectors for the above assigned vibrational modes.

Region C: photodetachment to the T_1 state of *o*- and *p*-methylenephenoxyl

The singlet–triplet splittings (ΔE_{ST}) for *o*- and *p*-methylenephenoxyl can also be measured. As previously mentioned, while the ground singlet state has a more stable resonance form, the excited triplet does not. Fig. 5 displays region C of the PES accessing the excited electronic states of the two isomers, obtained using the pulsed PES instrument with a photon energy of 3.494 eV. Again, the experimental data are colored black and red, while theoretical modeling is shown in green and purple. Peak A in the *o*-methylenephenoxide PES (top panel) is located at 2.752 ± 0.001 eV, which is 1.535 eV above the EA. Theoretical calculations (CBS-QB3) predict the first electronically excited triplet state to be 1.496 eV above the ground state, while the first electronically excited singlet state is over 3 eV higher in energy than the ground state. Given the experimental location of this peak in the spectrum, it is assigned as the transition from the anion vibronic ground state to the vibrational ground state of the first electronically excited triplet state of the neutral. This leads to a measurement of the T_1 electronic band origin, 2.752 ± 0.015 eV electron binding energy. Combining this value with the EA allows for a measurement of ΔE_{ST}(*o*-methylenephenoxyl) = 1.535 ± 0.019 eV, agreeing very well with the theoretically predicted energy difference (1.496 eV).

The vibrational transitions found within the electronic manifold may also be analyzed. Peak B is located 455 ± 10 cm^{-1} higher in binding energy relative to peak A. Theory predicts peak B to be dominated by excitation of two ring distortion vibrational modes with harmonic frequencies calculated to be ν_{32} = 456 cm^{-1} and ν_{29} = 530 cm^{-1}. Due to their proximity in frequency to each other, these two modes cannot be independently measured, and therefore we assign both transitions 32_0^1, 29_0^1 = 450 ± 160 cm^{-1}.

The *para* isomer also shows evidence of an excited electronic state vibrational progression. Some of the peaks in this spectrum are wider than the experimental resolution (by about a factor of 2) and there is an underlying continuum, some of which is extending from region B. Despite this, a theoretically predicted simulation still matches the observed spectrum quite well.

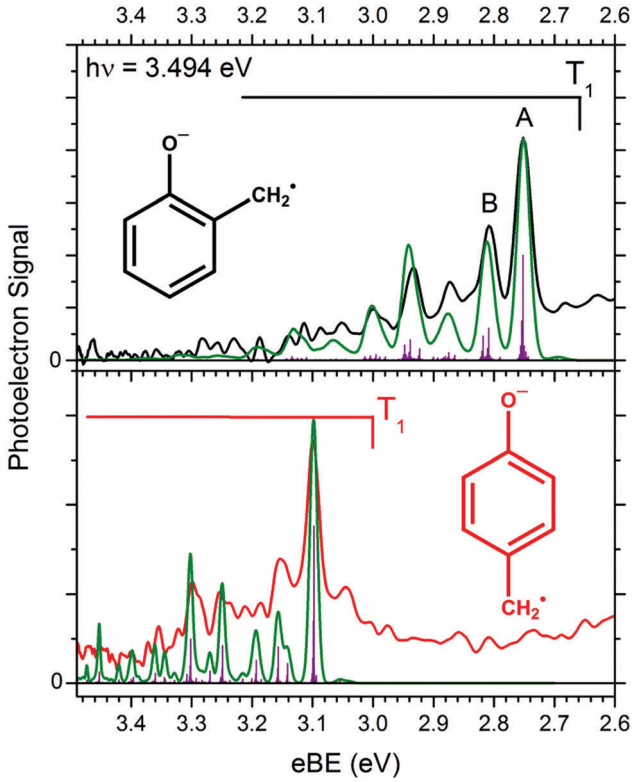

Fig. 5 Photoelectron spectra accessing the lowest triplet excited electronic states of the *o*- and *p*-methylenephenoxyl diradicals are shown in black and red traces, respectively. These spectra were collected with the pulsed PES instrument utilizing a photon energy of 3.494 eV. The calculated transitions and their corresponding Franck–Condon intensities are represented by purple sticks, while their convolutions with experimental resolution are shown in green.

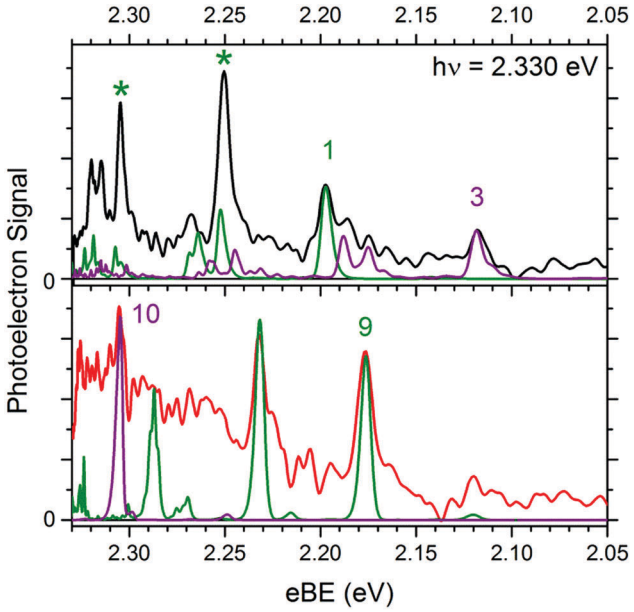

Fig. 6 Photoelectron spectra of m/z = 106, resulting from the reaction of O^- with *o*- (black) and *p*- (red) methylphenol, collected with the pulsed PES instrument with a photon energy of 2.330 eV. The numeric labels indicate the isomer listed in Fig. 2, and the asterisks are discussed in the text. The simulated PES, following their convolution with the experimental resolution, are shown in green and purple lines. The calculated transitions and their corresponding FCFs are shown in the ESI.†

The origin of the excited triplet state is measured to be 3.098 ± 0.010 eV. This results in a measured ΔE_{ST} = 2.002 ± 0.010 eV, which compares very well with the theoretically predicted 2.017 eV ΔE_{ST} splitting (CBS-QB3). No peaks can be definitively assigned to specific vibrational modes due to the spectral congestion, but once again, various ring distortion vibrations are responsible for the majority of the theoretically predicted Franck–Condon activity.

Region B: methylphenyloxide photoelectron spectra

Region B in Fig. 3 is now examined with higher resolution, using the VMI photoelectron spectrometer at a photon energy of 2.330 eV. These results are depicted in Fig. 6. Peaks 3 and 9 in region B in the PES for the *ortho* and *para* isomers are located at 2.118 and 2.177 eV binding energy, respectively. This eBE is very similar to electron detachment from methylphenoxide (EA = 2.1991 ± 0.0014 and 2.1199 ± 0.0014 eV for *ortho* and *para* isomers, respectively[46]), where the electron was located primarily on the oxygen moiety. Examining the energetic spacing between these peaks and peaks at higher binding energy in each isomer reveals energy differences of ~500 cm^{-1}, suggesting ring distortion vibrational excitation similar to that seen in regions A and C in the PES. From Fig. 1, it was observed that another anion structural isomer, likely to be methylphenyloxide anions, could result from the reaction of O^- with methylphenol. This would result in a radical site on the ring and the negative charge primarily located on the oxygen moiety, consistent with the observed eBE near 2 eV. Upon photodetachment, it is likely that the bond lengths and angles of the ring might change, leading to excitation of ring distortion vibrations, again consistent with the observations. Of course, there are multiple ring sites from which a hydrogen can be abstracted, leading to the anions shown in Fig. 2, which could result in significant spectral congestion due to several overlaid PES.

Theoretical predictions of the PES for the isomers in Fig. 2, along with the EAs of their corresponding neutrals, help to assign the observed peaks. Geometry optimization calculations performed here show that singlet diradicals with a hydrogen missing from a carbon in the ring will cause either the ring to open or significantly distort away from planarity, regardless of the site of abstraction. This type of structure is very different from the C_s symmetry (planar ring) of the distonic radical anion. A severely distorted ring structure in the neutral will result in very poor Franck–Condon overlap, and at best, an extended vibrational progression upon electron detachment would be observed. This is inconsistent with the experimental observations. The triplet state of the methylphenyloxyl neutral, however, maintains the planar ring structure and C_s symmetry similar to the anion, and detachment to this state would show a nearly vertical excitation spectrum, where the EA peak is one of the largest peaks in the progression. This is more consistent with the observations.

However, there are still a number of similar ring sites where a hydrogen could be abstracted. The most thermodynamically favorable methylphenyloxide anion is where the ring hydrogen is abstracted from the *meta* position relative to the oxide group. In a sequential reaction with O^- within an ion–molecule complex, methylphenoxide would be formed first, followed by the resulting OH then abstracting an additional H. The exothermicity for abstracting a ring hydrogen on methylphenoxide by OH is on the order of 2.4 kcal mol^{-1} (CBS-QB3). The corresponding triplet neutral diradicals of isomer anions 2, 4, and 10 in Fig. 2 have calculated EAs of 2.356 eV, 2.361 eV, and 2.273 eV, respectively. Other possible isomers would be anions 1, 3 and 9 in Fig. 2, whose corresponding triplet neutral diradicals have calculated EAs of 2.204 eV, 2.091 eV, and 2.137 eV, respectively. The reaction enthalpy for the ring hydrogen abstraction shows that formation of these anions is exothermic by approximately 1–2 kcal mol^{-1}. It should be noted that following the first step in the sequential reaction, a strongly activating substituent (such as O^- on methylphenoxide) typically favors electrophilic attacks onto the *ortho* and *para* positions, resulting in anions 1, 3, and 9 in Fig. 2. Regardless, all of the isomers in Fig. 2 could possibly be formed from the reaction of O^- with methylphenol.

The PES simulations for isomers whose corresponding triplet neutral diradicals have EAs predicted to be below 2.330 eV (namely, isomers 1, 3, 9, 10) are shown in Fig. 6 and compared with the experimental data. Note that only the PES simulations convolved with the experimental resolution are shown here (green and purple lines). The calculated transitions and their corresponding FCFs for both panels of Fig. 6 are shown in the ESI† (Fig. S8). The top panel shows that the photoelectron simulations of detachment from isomers 3 and 1 match the experimental spectrum fairly well. The calculations were shifted by 0.027 eV and 0.007 eV for the PES simulations of isomers 3 and 1, respectively, in order to match the experimental observations. Given the agreement between experiment and theory, the EAs of the neutral diradicals corresponding to anion isomers 3 and 1 are determined to be 2.118 ± 0.007 eV and 2.197 ± 0.006 eV, respectively. Note that there are some disagreements in the intensity of the FCFs for the PES of isomer 1, particularly above 2.25 eV. If the EA of the neutral diradical corresponding to isomer 1 were 2.25 eV instead of 2.118 eV, the simulation would still match the experiment fairly well, but this would leave the peak currently assigned as the EA unaccounted for in the simulation. Thus, it is more likely that there is a slightly larger geometry change between anion isomer 1 and its neutral triplet diradical than is currently predicted at this level of theory (BMK/6-311+G(3df,2p)). In particular, the intensities of the two peaks marked with asterisks (located at 2.250 and 2.305 eV) are less intense than predicted by the simulation, although only one dominant FCF is predicted to be responsible for these peaks. These two peaks are located 431 ± 30 and 867 ± 20 cm^{-1}, respectively, higher in binding energy than the EA. On comparison with theory, the transitions can be assigned to the fundamental and first overtone excitation in the ring distortion mode ν_{31} (calculated to be 441 cm^{-1}) in the triplet neutral diradical, leading to an experimental measurement of $31_0^1 = 430 \pm 80$ cm^{-1} and $31_0^2 = 870 \pm 80$ cm^{-1}. See the ESI† for the normal mode vectors for this vibrational mode. The other peaks in the spectrum are not clearly dominated by one or at most two transitions to warrant further vibrational assignments. In addition, the PES for isomers 2 and 4 are not observed with this photon energy (2.330 eV). In Fig. 3, use of a photon energy of 3.494 eV results in insufficient spectral resolution in region B to distinguish the PES for isomers 2 and 4. As a result, the EAs of the corresponding neutral molecules cannot be assigned.

In the bottom panel of Fig. 6, the photoelectron simulations for isomers 9 and 10 are seen to match the experimental observations fairly well, again following small shifts of 0.040 eV and 0.032 eV, respectively, to higher binding energy. Given the agreement between the experiment and theoretical predictions, the EAs of the neutral diradicals of isomers 9 and 10 are found to be 2.177 ± 0.006 eV and 2.305 ± 0.005 eV, respectively. As expected, the peaks observed in both experimental spectra are due to vibrational excitation of ring distortion modes upon photodetachment to the triplet neutral. However, given the spectral congestion apparent in the simulation combined with the overlapping spectra due to multiple isomers, no assignment of peaks to specific vibrational modes is possible.

Photoelectron spectrum of *m*-methylenephenoxide

The PES of *m*-methylenephenoxide proved more challenging to interpret, both experimentally and theoretically. Experimentally, no photoelectron signal was observed in region A, unlike in the PES for the other two isomers. This observation is consistent with the lack of the more stable singlet electronic state resonance form of cyclohexadienone that the *ortho* and *para* isomers possess. The majority of the photoelectron signal was observed in region B, with some additional signal in region C. There was a photon energy dependence of the signal observed when using 3.494 eV photon energy, as shown in Fig. S4 of the ESI.† As a result, 3.832 eV photon energy is used to obtain the results portrayed in Fig. 7. Additional PES are shown in the ESI,† using 3.494 eV and 2.330 eV photon energies. For region B, there appear to be possibly two progressions, with the peak near 2.2 eV marking the onset of the first progression, and the peak near 2.4 eV marking the start of the second progression. These onset energies are consistent with the predicted EA(*m*-methylenephenoxyl) of approximately 2 eV. Because of the possible spectral congestion in region B, calculations were necessary to aid in the PES interpretation.

Initial attempts at calculations not reported here showed inconsistency over a wide range of theoretical methods and basis sets, with large disparities in the EA(*m*-methylenephenoxyl), and sometimes large degrees of spin contamination and unphysical geometry optimizations. Throughout these calculations, however, the ground state of the *m*-methylenephenoxyl diradical was always the triplet state, in contrast to the other two isomers. As mentioned previously, the levels of theory that are employed in this work were chosen because of their previous success with other distonic radical anions and their diradical neutrals.[24,25] The EA of the triplet ground state of *m*-methylenephenoxyl is

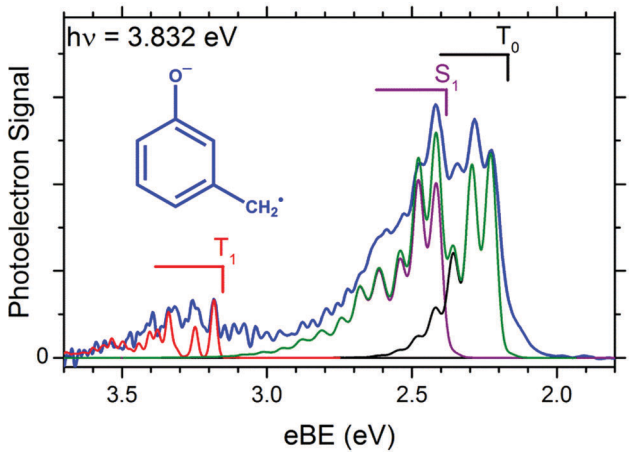

Fig. 7 Photoelectron spectra of m/z = 106, resulting from the reaction of O^- with *m*-methylphenol, collected with the pulsed PES instrument using a photon energy of 3.832 eV (blue trace). The PES simulations, convolved with the experimental resolution, are shown as black, purple, and red lines for transitions to the neutral T_0, S_1, and T_1 electronic states, respectively, from the ground state of the *m*-methylenephenoxide anion. The sum of the simulated PES in the 2–3 eV range is shown as the green line.

calculated (CBS-QB3) to be 2.186 eV, whereas the origin of the singlet excited state is 2.568 eV, 0.382 eV higher in energy than the triplet ground electronic state. Both of these electronic state origins, then, are predicted to be in region B of the experimental spectrum, which is consistent with the experimental observation of possibly two progressions in region B.

As seen in Fig. 7, the experimental spectrum is matched fairly well by the theoretically predicted simulation of photodetachment to form the triplet ground state and singlet excited state of neutral methylenephenoxyl diradical. Note that the simulations have been slightly shifted to best match the experimental spectrum, such that the T_0 origin, or the EA(*m*-methylenephenoxyl) = 2.227 ± 0.008 eV, and the S_1 origin is found at 2.418 ± 0.040 eV. The EA(*m*-methylenephenoxyl) was determined from a higher resolution experimental spectrum shown in Fig. S6 (ESI†), which uses 2.330 eV photon energy. Unfortunately, the S_1 origin is higher in energy than the 2.330 eV photon energy used in Fig. S6 (ESI†), so this lower resolution spectrum (Fig. 7) must be used to assign it, resulting in a larger error bar. The calculated transitions to the T_0 and S_1 states and associated FCFs are shown in Fig. S5 in the ESI.†

An added complication to the interpretation of the spectrum in region B is due to the possible presence of methylphenyloxide radical anions. For each possible methylphenyloxide isomer shown in Fig. 2, the corresponding triplet neutral species have EAs in the range of 2.1–2.5 eV. While thermodynamically the methylenephenoxide anion should be the most abundant, this does not rule out the presence of methylphenyloxide isomers. Indeed, in Fig. S6 (ESI†), an additional peak (near 2.27 eV) is observed in region B which is not accounted for by photodetachment to the T_0 state of the methylenephenoxyl diradical. This peak is very close to the calculated origin of the PES for isomers 5 (2.243 eV) and 8 (2.241 eV), but cannot be unambiguously assigned to either isomer due to the similarity in the calculated PES. The experimental spectra in both Fig. 7 and in the ESI† show several additional peaks in region B which are spaced by approximately 500 cm^{-1} from each other, consistent with the expected ring distortion vibrational excitation. However, the low experimental resolution and spectral congestion in this region of the spectrum does not allow for any vibrational mode assignments to be made.

The peaks seen in region C of the spectrum of the *meta* isomer span approximately 0.5 eV, with the start of the progression near 3.18 eV. The experimental spectrum shows several peaks in region C which are spaced by approximately 500 cm^{-1} from each other, again consistent with ring distortion vibrational excitation. Like the *ortho* and *para* isomers, region C is due to detachment to an excited electronic state of the neutral methylenephenoxyl radical. However, unlike these other isomers, *m*-methylenephenoxyl radical has several very low lying electronic states, all of which are accessible by the photon energy used here (3.832 eV). The T_0, S_1, T_1, and S_2 electronic states of *m*-methylenephenoxyl are calculated (TDDFT) to be within approximately 1 eV of each other, and therefore they are all accessible by the 3.832 eV photon energy. The second lowest lying excited state is the T_1 electronic state, which is predicted to have an EA near 3.19 eV, very close to the observed onset of the progression in region C. A simulated PES for the transition to the T_1 state of *m*-methylenephenoxyl is shown in Fig. 7 (red line), and matches the experimental spectrum very well. The experimental origin of the T_1 state is determined to be 3.182 eV ± 0.010 eV. There are a few peaks near 3.30 eV which are not accounted for by only detachment to the T_1 state of methylenephenoxyl. These could be due to detachment to the excited S_2 state, which is predicted to have a vertical detachment energy near 3.33 eV. The PES for detachment to the S_2 excited electronic state has not been simulated here due to TDDFT geometry optimization convergence problems. The calculated transitions to the T_1 state and associated FCFs are shown in Fig. S7 in the ESI.† Again, the spectral congestion in this region of the spectrum does not allow for any definitive vibrational mode assignments to be made.

Thermochemistry

The acid bracketing technique was used to determine the deprotonation enthalpy of the protonated forms of the three main anions studied in this work, namely *o*-, *m*-, and *p*-methylenephenol. These results were gathered with the FA-SIFT instrument and are combined with the other thermodynamic results presented in Tables 1 and 2. Using these data, experimental values for $\Delta_{acid}H^{\circ}_{298K}$ of the *o*-, *m*-, and *p*-methylenephenol radicals were found to be 341.4 ± 4.3, 349.1 ± 3.0, and 341.4 ± 4.3 kcal mol^{-1}, respectively. These were theoretically (CBS-QB3) predicted to be 342.1, 348.0, and 340.6 kcal mol^{-1}, respectively. This comparison assumes that the protonation site of the distonic radical anions in the experiment was the oxygen atom, and the close agreement with the experimental results corroborates this assumption. Protonation on the CH_2 site was also modeled, but those predictions fell outside the experimental error bars by >10 kcal mol^{-1}, and were therefore discounted.

Table 1 Summary of acid bracketing results. A "+" denotes an exothermic proton transfer occurred, while a "−" denotes its absence. All acidities and deprotonation enthalpies are taken from the NIST Chemistry Reference Database[73]

Reference acid	$\Delta_{acid}G^{\circ}_{298K}$ (kcal mol^{-1})	$\Delta_{acid}H^{\circ}_{298K}$ (kcal mol^{-1})	*o*-Methylenephenoxide	*m*-Methylenephenoxide	*p*-Methylenephenoxide
p-Trifluoromethylphenol	330.1 ± 1.9	337.0 ± 2.2	+	+	+
3-Mercaptopropionic acid	332.4 ± 1.9	339.4 ± 2.2	+	+	+
o-Chlorophenol	337.1 ± 1.9	343.4 ± 2.4	−	+	−
p-Fluorophenol	339.9 ± 1.9	346.8 ± 2.2	−	+	−
Propionic acid	340.4 ± 2.0	347.4 ± 2.2	−	+	−
Acetic acid	341.1 ± 2.0	348.1 ± 2.2	−	+	−
Phenol	342.3 ± 2.0	350.0 ± 2.0	−	−	−
2,2,3,3,3-Pentafluoro-1-propanol	348.8 ± 6.0	355.4 ± 6.1	−	−	−

Table 2 Summary of results for methylenephenoxyl radicals. Measured values are displayed in plain text while calculated values are in italics. The two structures for the *ortho* and *para* isomers show the more stable singlet ground state of the substituted cyclohexadienone as well as the triplet diradical excited state

	EA/eV	ΔE_{ST}/eV	$\Delta_{acid}H^{\circ}_{298K}$[a]/kcal mol^{-1}	BDE[a]/kcal mol^{-1}
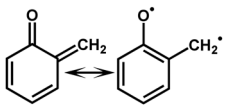	1.217 ± 0.012 *1.295*[b]	1.535 ± 0.019 *1.496*[b]	341.4 ± 4.3 *342.1*[b]	55 ± 5 *57.2*[b]
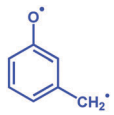	2.227 ± 0.008[c] *2.186*[b,c]	−0.191 ± 0.040 *−0.382*[b]	349.1 ± 3.0 *348.0*[b]	86 ± 4 *83.6*[b]
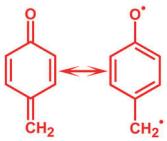	1.096 ± 0.007 *1.211*[b]	2.002 ± 0.010 *2.017*[b]	341.4 ± 4.3 *340.6*[b]	52 ± 5 *53.6*[b]

[a] Refers to O–H bond of the corresponding methylenephenol radical, forming singlet substituted cyclohexadienone, or triplet methylenephenoxyl for the *meta* isomer. [b] Calculated values using CBS-QB3 composite method. [c] Refers to the triplet ground electronic state of *m*-methylenephenoxyl radical.

The experimental determination of the deprotonation enthalpies and the EAs of *o*-, *m*-, and *p*- methylenephenoxyl enables a determination of the O–H bond strength in the methylenephenol radical isomers in the gas phase, *via* a thermochemical cycle.[66] The experimental values for the deprotonation enthalpies were adjusted to their 0 K values using the calculated heat capacities at constant pressure, C_p.[46] The dissociation energies were derived to be 55 ± 5, 86 ± 4, and 52 ± 5 kcal mol^{-1} for *o*-, *m*-, and *p*-methylenephenol, respectively. These are similar to the theoretical bond dissociation energies of 57.2, 83.6, and 53.6 kcal mol^{-1}, respectively.

V. Discussion

In general, the experimental PES for all three isomers of methylenephenoxide were well reproduced by theoretical predictions, and a summary of some of these results can be found in Table 2. PES signatures belonging to additional isomers (methylphenyloxide) were found to be present in the experimental data, which was particularly important in explaining the experimental observations in region B of the spectra. See Table 3 for this additional summary of results. The EAs of the methylenephenoxyl diradicals measured in this work can be compared to the deprotonated methylphenols, studied previously, in order to gain additional physical insight.[46] The EAs for the *o*-, *m*-, and *p*-methylphenoxyl radicals are 2.1991 ± 0.0014, 2.2177 ± 0.0014,

Table 3 Summary of results for the triplet ground electronic states of methylphenyloxyl radicals. Measured values are displayed in plain text while calculated values (CBS-QB3) are in italics

	EA/eV		EA/eV
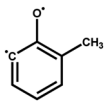	2.197 ± 0.006 *2.204*	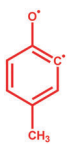	2.177 ± 0.006 *2.137*
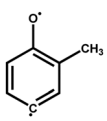	2.118 ± 0.007 *2.186*	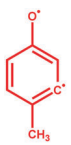	2.305 ± 0.005 *2.273*

and 2.1199 ± 0.0014 eV, respectively. The *o*- and *p*-methylenephenoxyl diradicals have an EA of ~1 eV, while *m*-methylenephenoxide and the methylphenoxyl radicals all have EAs of ~2 eV. As initially predicted, this discrepancy is most likely due to an increased stabilization of the neutral *o*- and *p*-methylenephenoxyl diradicals in their ground singlet electronic state relative to the anion due to their more stable resonance forms of 6-methylene-2,4-cyclohexadien-1-one and 4-methylene-2,5-cyclohexadien-1-one.

While the ground singlet electronic states for the *ortho* and *para* isomers benefit from the stable resonance form, their excited triplet states do not since the radical electrons are in orbitals in the plane of the benzene ring, and are unable to conjugate with the aromatic π system. Thus, the ΔE_{ST} in the *o*- and *p*-methylenephenoxyl diradicals are fairly large, at 1.535 ± 0.019 and 2.002 ± 0.010 eV, respectively. While the large ΔE_{ST} values for *ortho* and *para* isomers are reasonable given the stable cyclohexadienone form of the singlet state, the larger ΔE_{ST} for the *para* isomer compared to the *ortho* isomer is somewhat surprising. For the benzyne diradical,[67] relatively small ΔE_{ST} were observed, where *p*-benzyne was found to have ΔE_{ST} = 0.167 ± 0.016 eV. As the two radical sites were brought closer together, *i.e.* starting with *p*-, then *m*-, and finally *o*-benzyne, the ΔE_{ST} monotonically increased from 0.167 ± 0.016 to 1.628 ± 0.013 eV. This is expected to occur because the coupling between the two radical electrons would increase as they come into closer spatial proximity with one another, thus translating the singlet and triplet states further apart in energy. In the methylenephenoxyl diradicals, this is not the case. Perhaps the added complication of the O···CH_2 interaction in the *ortho* isomer and/or the increased symmetry of the *para* isomer is significant in this respect. The *meta* isomer has the smallest ΔE_{ST} = −0.191 eV, where the triplet state is lower in energy than the singlet state, which is consistent with Hund's rule for maximum multiplicity.

The O–H bond strengths of the methylenephenol radical isomers can be derived from the other thermochemical values, and these are summarized in Table 2. The O–H bond strength of the *m*-methylenephenol isomer (86 ± 4 kcal mol^{-1}) is the same within error as that reported recently for *m*-methylphenol (86.53 ± 0.14 kcal mol^{-1}).[38,68] This suggests that the presence of a methylene radical instead of a methyl group in the *meta* position has very little, if any, influence on the O–H bond strength. For the *o*- and *p*-methylenephenol, the O–H bond strengths are significantly reduced, measuring only 55 ± 5 kcal mol^{-1} and 52 ± 5 kcal mol^{-1}, respectively. This can be compared to the O–H bond strengths for *o*- and *p*-methylphenol,[38,68] which are approximately 84 kcal mol^{-1}. This suggests that the substituted cyclohexadienone products formed following the O–H bond dissociation of *o*- and *p*-methylenephenol are stabilized relative to the diradical form by an approximate 30 kcal mol^{-1}.

There remain several disparities between the experimental results and the theoretically predicted PES that are common across all of the PES reported here. First, at higher binding energies, the predicted peak positions tend to be higher in energy compared to the experiment. This is most likely due to anharmonicity effects, which were not included in the Frank–Condon simulations. Second, there is typically more broadening than can be explained by experimental resolution or predicted spectral congestion. One might consider if rotational broadening could explain this, but the predicted changes in the rotational constants for all the isomers considered here are <0.01 cm^{-1}, making this an unlikely contribution to the observed broadening.[69] Such extensive broadenings in larger aromatic and/or diradical compounds have been frequently observed previously.[11,16,27] Third, a photon energy dependence of the *ortho* and *meta* PES was observed and these spectra are shown in the ESI.† This is particularly obvious for the *meta* isomer (Fig. S4, ESI†), where some peaks attributed to the S_1 state noticeably change intensity when using 3.494 eV *versus* 3.832 eV photon energy. This phenomenon is attributed to electron autodetachment, which has been a hallmark in similar aromatic species.[46,70–72] It should also be noted that some of the additional line broadening was observed to have a photon energy dependence. Thus, electron autodetachment is one possible reason for the disagreement with our simulations, which do not take such phenomena into account.

VI. Conclusions

The photoelectron spectra of the distonic radical anions *o*-, *m*-, and *p*-methylenephenoxide have been studied. The EAs of the corresponding neutrals were measured to be 1.217 ± 0.012, 2.227 ± 0.008, and 1.096 ± 0.007 eV, respectively. Upon photodetachment, vibrational ring distortion modes were shown to be Franck–Condon active and have measured frequencies of 570 ± 180 and 450 ± 80 cm^{-1} for the *ortho* and *para* isomers' neutral singlet ground electronic states. Photodetachment to the electronically excited states was also investigated and similar vibrational modes were found to be Franck–Condon active. Detachment to the excited triplet state of the *ortho* isomer showed excitation of ring distortion vibrational modes with a measured frequency of 450 ± 160 cm^{-1}. Additional anions (methylphenyloxides) were observed to be formed following the abstraction of ($H + H^+$) from methylphenol by reaction with O^-. Although the photoelectron spectra of these methylphenyloxides were spectrally congested due to overlapping spectra, several EAs of their corresponding neutrals were measured. The thermochemistry of these molecules was also investigated using flowing afterglow-selected ion flow tube mass spectrometry in conjunction with the acid bracketing technique, yielding deprotonation enthalpies for the *o*-, *m*-, and *p*-methylenephenol radical anions to be 341.4 ± 4.3, 349.1 ± 3.0, and 341.4 ± 4.3 kcal mol^{-1}, respectively. Construction of a thermodynamic cycle allowed for an experimental determination of the relatively weak bond dissociation energy of the O–H bond for the *ortho* and *para* methylenephenol isomers to be 55 ± 5, and 52 ± 5 kcal mol^{-1}, respectively. The *m*-methylenephenol isomer has a stronger O–H bond, 86 ± 4 kcal mol^{-1}, which is very similar to the O–H bond strength in *m*-methylphenol. Most of the observed trends regarding the EAs and thermochemistry

can be explained by the significant stabilization of the ground singlet electronic state of the *ortho* and *para* isomers brought about by the formation of a substituted cyclohexadienone rather than a diradical.

Conflicts of interest

The authors declare no competing financial interest.

Acknowledgements

W. C. L. gratefully acknowledges support from NSF (Grant No. PHY1734006 and CHE1213862) for significant contributions to this project. J. H. L. also gratefully acknowledges support from Marie Skłodowska Curie Actions Individual Fellowship (MSCA-IF, Horizon 2020 Grant No. 743642). V. M. B. gratefully acknowledges support from NSF (Grant No. CHE1300886).

References

1 M. Bendikov, H. M. Duong, K. Starkey, K. N. Houk, E. A. Carter and F. Wudl, *J. Am. Chem. Soc.*, 2004, **126**, 7416–7417.
2 *Diradicals*, ed. W. T. Borden, John Wiley and Sons, New York, 1982.
3 B. Breiner, K. Kaya, S. Roy, W.-Y. Yang and I. V. Alabugin, *Org. Biomol. Chem.*, 2012, **10**, 3974–3987.
4 D. Doehnert and J. Koutecky, *J. Am. Chem. Soc.*, 1980, **102**, 1789–1796.
5 H. K. Hall and A. B. Padias, *Acc. Chem. Res.*, 1990, **23**, 3–9.
6 R. Hoffmann, D. B. Boyd and S. Z. Goldberg, *J. Am. Chem. Soc.*, 1970, **92**, 3929–3936.
7 K. N. Houk, J. Liu, N. C. DeMello and K. R. Condroski, *J. Am. Chem. Soc.*, 1997, **119**, 10147–10152.
8 R. Huisgen, *J. Org. Chem.*, 1976, **41**, 403–419.
9 P. G. Wenthold and R. R. Squires, *J. Am. Chem. Soc.*, 1994, **116**, 6401–6412.
10 A. R. Luxon, N. Orms, R. Kanters, A. I. Krylov and C. A. Parish, *J. Phys. Chem. A*, 2018, **122**, 420–430.
11 G. E. Davico, R. L. Schwartz, T. M. Ramond and W. C. Lineberger, *J. Am. Chem. Soc.*, 1999, **121**, 6047–6054.
12 E. Goldstein, B. Beno and K. N. Houk, *J. Am. Chem. Soc.*, 1996, **118**, 6036–6043.
13 J. Gräfenstein, A. M. Hjerpe, E. Kraka and D. Cremer, *J. Phys. Chem. A*, 2000, **104**, 1748–1761.
14 L. Koziol, V. A. Mozhayskiy, B. J. Braams, J. M. Bowman and A. I. Krylov, *J. Phys. Chem. A*, 2009, **113**, 7802–7809.
15 R. Lindh, T. J. Lee, A. Bernhardsson, B. J. Persson and G. Karlstroem, *J. Am. Chem. Soc.*, 1995, **117**, 7186–7194.
16 W. C. Lineberger and W. T. Borden, *Phys. Chem. Chem. Phys.*, 2011, **13**, 11792–11813.
17 A. Rajca, *Chem. Rev.*, 1994, **94**, 871–893.
18 E. Ramos-Cordoba and P. Salvador, *Phys. Chem. Chem. Phys.*, 2014, **16**, 9565–9571.
19 V. Vanovschi, A. Krylov and P. Wenthold, *Theor. Chem. Acc.*, 2008, **120**, 45–58.
20 G. P. F. Wood, L. Radom, G. A. Petersson, E. C. Barnes, M. J. Frisch and J. A. Montgomery, *J. Chem. Phys.*, 2006, **125**, 094106.
21 X. Asensio, À. González-Lafont, J. Marquet, J. M. Lluch and M. Geoffroy, *J. Mol. Struct.*, 2009, **913**, 228–235.
22 M. Born, S. Ingemann and N. M. M. Nibbering, *Mass Spectrom. Rev.*, 1997, **16**, 181–200.
23 S. Gronert, *Chem. Rev.*, 2001, **101**, 329–360.
24 G. Gryn'ova and M. L. Coote, *J. Am. Chem. Soc.*, 2013, **135**, 15392–15403.
25 G. Gryn'ova, D. L. Marshall, S. J. Blanksby and M. L. Coote, *Nat. Chem.*, 2013, **5**, 474–481.
26 B. T. Hill, J. C. Poutsma, L. J. Chyall, J. Hu and R. R. Squires, *J. Am. Soc. Mass Spectrom*, 1999, **10**, 896–906.
27 T. Ichino, S. M. Villano, A. J. Gianola, D. J. Goebbert, L. Velarde, A. Sanov, S. J. Blanksby, X. Zhou, D. A. Hrovat, W. T. Borden and W. C. Lineberger, *J. Phys. Chem. A*, 2011, **115**, 1634–1649.
28 M. Lin and J. J. Grabowski, *Int. J. Mass Spectrom.*, 2004, **237**, 149–165.
29 D. C. Magri and M. S. Workentin, *Chem. – Eur. J.*, 2008, **14**, 1698–1709.
30 K. K. Morishetti, P. Sripadi, V. Mariappanadar and J. Ren, *Int. J. Mass Spectrom.*, 2011, **299**, 169–177.
31 K. Pius and J. Chandrasekhar, *J. Chem. Soc., Perkin Trans. 2*, 1988, 1291–1295.
32 D. R. Reed, M. Hare and S. R. Kass, *J. Am. Chem. Soc.*, 2000, **122**, 10689–10696.
33 D. R. Reed, M. C. Hare, A. Fattahi, G. Chung, M. S. Gordon and S. R. Kass, *J. Am. Chem. Soc.*, 2003, **125**, 4643–4651.
34 K. M. Stirk, L. K. M. Kiminkinen and H. I. Kenttamaa, *Chem. Rev.*, 1992, **92**, 1649–1665.
35 N. R. Wijeratne and P. G. Wenthold, *J. Am. Soc. Mass Spectrom*, 2007, **18**, 2014–2016.
36 M. Fujio, R. T. McIver and R. W. Taft, *J. Am. Chem. Soc.*, 1981, **103**, 4017–4029.
37 D. J. Hopper, *Biochem. J.*, 1978, **175**, 345–347.
38 G. A. King, A. L. Devine, M. G. D. Nix, D. E. Kelly and M. N. R. Ashfold, *Phys. Chem. Chem. Phys.*, 2008, **10**, 6417–6429.
39 K. P. Krishnan Namboodiri, S. Viswanathan, R. Ganesan and V. C. Jyothi Bhasu, *Monatsh. Chem. Chem. Mon.*, 1982, **113**, 949–963.
40 X. Liu, M. Liu, X. Guo and J. Zhou, *Catal. Commun.*, 2008, **9**, 1–7.
41 L. Nie, P. M. de Souza, F. B. Noronha, W. An, T. Sooknoi and D. E. Resasco, *J. Mol. Catal. A: Chem.*, 2014, **388–389**, 47–55.
42 W. T. Read, *Industrial Chemistry*, Chapman and Hall, Limited, London, 1947.
43 L. S. Richard, C. E. S. Bernardes, H. P. Diogo, J. P. Leal and M. E. Minas da Piedade, *J. Phys. Chem. A*, 2007, **111**, 8741–8748.
44 E. S. Simon, P. G. Papoulias and P. C. Andrews, *Rapid Commun. Mass Spectrom.*, 2013, **27**, 1619–1630.
45 C.-M. Tseng, Y. T. Lee, C.-K. Ni and J.-L. Chang, *J. Phys. Chem. A*, 2007, **111**, 6674–6678.

46 D. J. Nelson, W. K. Gichuhi, E. M. Miller, J. H. Lehman and W. C. Lineberger, *J. Chem. Phys.*, 2017, **146**, 074302.
47 M. A. Kurinovich and J. K. Lee, *J. Am. Soc. Mass Spectrom.*, 2002, **13**, 985–995.
48 D. G. Leopold, K. K. Murray, A. E. S. Miller and W. C. Lineberger, *J. Chem. Phys.*, 1985, **83**, 4849–4865.
49 J. M. Van Doren, S. E. Barlow, C. H. DePuy and V. M. Bierbaum, *Int. J. Mass Spectrom. Ion Processes*, 1987, **81**, 85–100.
50 K. M. Ervin, J. Ho and W. C. Lineberger, *J. Phys. Chem.*, 1988, **92**, 5405–5412.
51 Y.-J. Lu, J. H. Lehman and W. C. Lineberger, *J. Chem. Phys.*, 2015, **142**, 044201.
52 A. T. J. B. Eppink and D. H. Parker, *Rev. Sci. Instrum.*, 1997, **68**, 3477–3484.
53 L. Sheps, E. M. Miller and W. C. Lineberger, *J. Chem. Phys.*, 2009, **131**, 064304.
54 B. Ruscic, A. F. Wagner, L. B. Harding, R. L. Asher, D. Feller, D. A. Dixon, K. A. Peterson, Y. Song, X. Qian, C.-Y. Ng, J. Liu, W. Chen and D. W. Schwenke, *J. Phys. Chem. A*, 2002, **106**, 2727–2747.
55 V. Dribinski, A. Ossadtchi, V. A. Mandelshtam and H. Reisler, *Rev. Sci. Instrum.*, 2002, **73**, 2634–2642.
56 H. Hotop and W. C. Lineberger, *J. Phys. Chem. Ref. Data*, 1985, **14**, 731–750.
57 C. Blondel, W. Chaibi, C. Delsart, C. Drag, F. Goldfarb and S. Kröger, *Eur. Phys. J. D*, 2005, **33**, 335–342.
58 J. Cooper and R. N. Zare, *J. Chem. Phys.*, 1968, **48**, 942–943.
59 K. M. Ervin, I. Anusiewicz, P. Skurski, J. Simons and W. C. Lineberger, *J. Phys. Chem. A*, 2003, **107**, 8521–8529.
60 D. M. Neumark, K. R. Lykke, T. Andersen and W. C. Lineberger, *Phys. Rev. A: At., Mol., Opt. Phys.*, 1985, **32**, 1890–1892.
61 M. J. Frisch, G. W. Trucks, H. B. Schlegel, G. E. Scuseria, M. A. Robb, J. R. Cheeseman, G. Scalmani, V. Barone, B. Mennucci, G. A. Petersson, H. Nakatsuji, M. Caricato, X. Li, H. P. Hratchian, A. F. Izmaylov, J. Bloino, G. Zheng, J. L. Sonnenberg, M. Hada, M. Ehara, K. Toyota, R. Fukuda, J. Hasegawa, M. Ishida, T. Nakajima, Y. Honda, O. Kitao, H. Nakai, T. Vreven, J. A. Montgomery Jr., J. E. Peralta, F. Ogliaro, M. J. Bearpark, J. Heyd, E. N. Brothers, K. N. Kudin, V. N. Staroverov, R. Kobayashi, J. Normand, K. Raghavachari, A. P. Rendell, J. C. Burant, S. S. Iyengar, J. Tomasi, M. Cossi, N. Rega, N. J. Millam, M. Klene, J. E. Knox, J. B. Cross, V. Bakken, C. Adamo, J. Jaramillo, R. Gomperts, R. E. Stratmann, O. Yazyev, A. J. Austin, R. Cammi, C. Pomelli, J. W. Ochterski, R. L. Martin, K. Morokuma, V. G. Zakrzewski, G. A. Voth, P. Salvador, J. J. Dannenberg, S. Dapprich, A. D. Daniels, Ö. Farkas, J. B. Foresman, J. V. Ortiz, J. Cioslowski and D. J. Fox, *Gaussian 09 (Revision B)*, Gaussian, Inc., Wallingford, CT, USA, 2009.
62 K. M. Ervin, T. M. Ramond, G. E. Davico, R. L. Schwartz, S. M. Casey and W. C. Lineberger, *J. Phys. Chem. A*, 2001, **105**, 10822–10831.
63 T. E. Sharp and H. M. Rosenstock, *J. Chem. Phys.*, 1964, **41**, 3453–3463.
64 P. Chen, *Unimolecular and Bimolecular Reactions Dynamics*, John Wiley & Sons, ChinChester, 1994.
65 E. B. Wilson, *Phys. Rev.*, 1934, **45**, 706–714.
66 K. M. Ervin and V. F. DeTuri, *J. Phys. Chem. A*, 2002, **106**, 9947–9956.
67 P. G. Wenthold, R. R. Squires and W. C. Lineberger, *J. Am. Chem. Soc.*, 1998, **120**, 5279–5290.
68 T. N. V. Karsili, A. M. Wenge, B. Marchetti and M. N. R. Ashfold, *Phys. Chem. Chem. Phys.*, 2014, **16**, 588–598.
69 M. J. Travers, D. C. Cowles, E. P. Clifford, G. B. Ellison and P. C. Engelking, *J. Chem. Phys.*, 1999, **111**, 5349–5360.
70 R. F. Gunion, M. K. Gilles, M. L. Polak and W. C. Lineberger, *Int. J. Mass Spectrom. Ion Processes*, 1992, **117**, 601–620.
71 H.-T. Liu, C.-G. Ning, D.-L. Huang, P. D. Dau and L.-S. Wang, *Angew. Chem., Int. Ed.*, 2013, **52**, 8976–8979.
72 D.-L. Huang, H.-T. Liu, C.-G. Ning and L.-S. Wang, *J. Chem. Phys.*, 2015, **142**, 124309.
73 *Thermochemical Data in NIST Chemistry WebBook, NIST Standard Reference Database Number 69*, ed. P. J. Linstrom and W. G. Mallard, http://webbook.nist.gov/chemistry/, accessed August 2018.

